Structural Engineering and Mechanics, *Vol. 71, No. 3 (2019) 211-221*
DOI: https://doi.org/10.12989/sem.2019.71.3.211

Research on eccentric compression of ultra-high performance fiber reinforced concrete columns

Kaize Ma*, Yudong Ma[a] and Boquan Liu[b]

Department of Civil Engineering, Chang'an University, 201 Yanta Road, Xi'an, China

(Received February 18, 2019, Revised March 28, 2019, Accepted March 30, 2019)

Abstract. To study the eccentric compression behavior of ultra-high performance fiber reinforced concrete (UHPFRC) columns, six UHPFRC columns and one high-strength concrete (HSC) column were tested. Variation parameters include load eccentricity, volume of steel fibers and stirrup ratio. The crack pattern, failure mode, bearing capacity, and deformation of the specimens were studied. The results showed that the UHPFRC columns had different failure modes. The large eccentric compression failure mode was the longitudinal tensile reinforcements yielded and many horizontal cracks appeared in the tension zone. The small eccentric compression failure mode was the longitudinal compressive reinforcements yielded and vertical cracks appeared in the compressive zone. Because of the bridging effect of steel fibers, the number of cracks significantly increased, and the width of cracks decreased. The load-deflection curves of the UHPFRC columns showed gradually descending without sudden dropping, indicating that the specimens had better deformation. The finite element (FE) analysis was performed to stimulate the damage process of the specimens with monotonic loading. The concrete damaged plasticity (CDP) model was adopted to characterize the behaviour of UHPFRC. The contribution of the UHPFRC tensile strength was considered in the bearing capacity, and the theoretical calculation formulas were derived. The theoretical calculation results were consistent with the test results. This research can provide the experimental and theoretical basis for UHPFRC columns in engineering applications.

Keywords: ultra-high performance fiber reinforced concrete; eccentric compression column; failure mode; bearing capacity; deformation; finite element (FE) analysis

1. Introduction

Ultra-high performance fiber reinforced concrete (UHPFRC) is a new type of cement-based composite material that has been developed in recent decades (Richard and Cheyrezy, 1995, Rossi, 2001, Yoo and Yoon, 2016).The main features of UHPFRC are ultra-high compressive strength and hardening post-crack behavior in tension (Habel *et al.* 2006, Graybeal, 2007, Su *et al.* 2017, Hu *et al.* 2018).UHPFRC is mainly characterized by high packing density and low water-cementitious materials ratio (*w/c*) that can be as low as 0.14 (Larrard and Sedran 1994). The high packing density is achieved by eliminating the use of coarse aggregate and by using other fine and cementitious materials with high fineness such as ground silica. Moreover, the addition of short, discontinuous steel fibers greatly enhances the tensile and flexural behaviors of UHPFRC (Kazemi and Lubell, 2012, Wu *et al.* 2016). The compressive and tensile strength of UHPFRC was significantly affected by the volume and aspect ratio of steel fibers (Hoang and Fehling, 2017). To increase compressive strength, intensive studies were conducted mostly with the application of specific material and treatments, such as vacuum mixing, hot temperature and high-pressure techniques (Heinz and Ludwig, 2004, Schachinger *et al.* 2008, Magureanu *et al.* 2012, and Premet *et al.* 2015). Compared to apply heat and pressure treatment, the UHPFRC was manufactured using conventional materials and production methods. The cement was replaced with fly ash (FA), ground granulated blast-furnace slag (GGBS) and limestone powder. The results showed that the compressive strengths of UHPFRC were in the range of 120-150 MPa (Wang *et al.* 2012, Yu *et al.* 2015, and Alsalman *et al.* 2017). Many countries have provided the design guidelines of UHPFRC (AFGC, 2013, CSTCC, 2015, JSCE, 2006, KCI, 2012). Several researchers studied the flexural behavior of UHPFRC beams. The beams exhibited ductile failure, and the cracks were denser and finer. The steel fibers could effectively resist the widening of the cracks (Chen *et al.* 2017, Singh *et al.* 2017, Qi *et al.* 2017, Yang *et al.* 2012, Yoo and Yoon, 2015). In addition, Singh, *et al.* (2017) established the numerical models of UHPFRC beams, which were successfully validated with the test results. Safdar *et al.* (2016), Al-Osta *et al.* (2017) and Murthy *et al.* (2018) investigated reinforced concrete beams were repaired with varying thicknesses of UHPFRC in the tension and compression zone. The results showed that the flexural strengths of the beams were improved with the increase of UHPFRC thickness. Hosinieh *et al.* (2015) and Shin *et al.* (2017) tested the performance of UHPFRC columns under axial forces. The steel fibers could

*Corresponding author, Associate Professor
E-mail: makaize@chd.edu.cn
[a] Graduate student
E-mail: yudongma@sohu.com
[b] Professor
E-mail: bqliu@chd.edu.cn

ISSN: 1225-4568 (Print), 1598-6217 (Online)

significantly improve the bearing capacity, deformation of UHPFRC columns. When the columns were damaged, the protective cover did not easily spall. Xu *et al.* (2017) tested 14 UHPFRC columns subjected to quasi-static cyclic loading. The results showed that the failure modes were flexural, flexural-shear, and shear failure. The cracking of concrete and bulking of longitudinal reinforcements were efficiently delayed due to the steel fibers. Owing to its excellent mechanical properties, UHPFRC has been attractive to use in civil infrastructures (Fehling *et al.* 2014, Russell and Graybeal, 2013).

The overall enhanced properties of UHPFRC contribute to the majorization of the total performance of columns, which improved the bearing capacity, the deformation capacity and the seismic performance, and reduced the damage degree, the stiffness degradation rate and the amount of concrete used. Based on the higher performance of UHPFRC column, numerous advantages of structural in terms of durability, ductility, workability, sustainability and aesthetic are improved. However, there are limited previous studies on the behavior of UHPFRC columns under eccentric loads. In order to investigate the eccentric compression behavior of UHPFRC columns, the research firstly analyzed the mechanical properties of UHPFRC with different volumes of steel fibers. Then, six UHPFRC columns and one high-strength concrete (HSC) column with the variation parameters of load eccentricity, volume of steel fibers and stirrup ratio were tested. An advanced FE analysis was used to stimulate damage process, and provided a reliable method for the establishment of a numerical model of UHPFRC column. Based on the results, the formulas were derived to calculate the bearing capacity of eccentric compression UHPFRC columns, which was expected to provide some reference for engineering design.

2 Material research

2.1 Material proportions

Based on the optimum packing density of the particles material gradation, the UHPFRC with different volumes of steel fibers have been researched. The Portland cement was type P.I 52.5, with compressive strength of 58.5MPa. Silica fume, fly ash, and slag were used as the supplementary cementitious material. Superfine river sand belonged to local area was used as fine aggregate. The particle size distribution of the used material was shown in Fig.1. The super-plasticizer was used in the mixture to achieve the required workability. The steel fibers with tensile strength of 2,000 MPa, a diameter of 0.2 mm, and a length of 13 mm were used. The mixture designs of UHPFRC with different volumes of steel fibers are shown in Table 1. The volumes of steel fibers were 0.5%, 1%, 1.5%, 2%, 2.5%, and 3%, and the weight of steel fibers was 39 kg, 78 kg, 117 kg, 156 kg, 195 kg, and 234 kg, respectively.

Cement, silica fume, fly ash, slag, and superfine river sand were premixed for three minutes to produce flowable UHPFRC. Water mixed with super-plasticizer was then poured into the dry mixture and stir for four minutes. The steel fibers were quickly and evenly dispersed into the

Table 1 Material proportions

Groups	Water (kg/m^3)	Cement (kg/m^3)	Silica fume (kg/m^3)	Fly ash (kg/m^3)	Slag (kg/m3)	Fine sand (kg/m^3)	Super plasticizer (kg/m^3)	Steel fibers (kg/m^3)
UHPFRC0	205.1	603	241	180.9	180.9	965	24.1	0
UHPFRC1	205.1	603	241	180.9	180.9	965	24.1	39
UHPFRC2	205.1	603	241	180.9	180.9	965	24.1	78
UHPFRC3	205.1	603	241	180.9	180.9	965	24.1	117
UHPFRC4	205.1	603	241	180.9	180.9	965	24.1	156
UHPFRC5	205.1	603	241	180.9	180.9	965	24.1	194
UHPFRC6	205.1	603	241	180.9	180.9	965	24.1	234

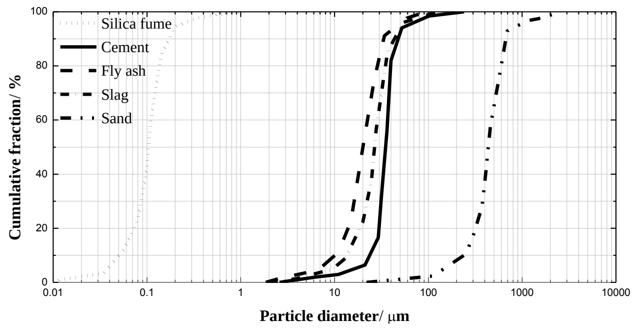

Fig. 1 Particle size distribution of the used material

mixture within thirty seconds and then stir for another three minutes. At last, the UHPFRC was cast in molds from the center, and vibrated with a vibration table for one minute. The UHPFRC specimens were removed from the molds after 24h later, and placed in a standard curing room with temperature and humidity of 20 ± 2^0 and $\geq 95\%$ for 27 days in this study.

2.2 Results analysis

A flow table test was used to measure the flowability of UHPFRC, and the test values of UHPFRC are shown in Table 2. The UHPFRC achieved a good flowability as the volume of steel fibers was 2%. The test values of UHPFRC4 decreased by 16% compared with UHPFRC2, and sharply decreased to 192 mm as the volume of steel fibers increased to 3%. The steel fibers significantly affected the flowability of UHPFRC.

For the compressive test, the cube specimens with dimensions of $100 \times 100 \times 100$ mm were used. The load was applied by a universal testing machine (UTM), which has the load capacity up to 2000 kN, with the loading rate of 0.001mm/minute. The steel fibers had a bridge effect during the UHPFRC compressive test that contributed to micro-cracking development. UHPFRC specimens remained in one piece after tests. The compressive strengths of UHPFRC mixtures are shown in Table 2. The volume of steel fibers varied between 0 and 3%, the UHPFRC had a high compressive strength, from 105.3 MPa to 145.2 MPa. The continuous increase in the volume of steel fibers improved the compressive strength. But the growth ratio of compressive strength decreased after the volume of steel fibers rose to 2%. The presence of fibers can prevent the explosive failure and held the concrete together after the cube specimen was crushed in compression.

The dog-bone specimens were used in the direct tension tests, with the mid-span section of 50 ×25 mm, the end section of 90×25 mm, the total length of 300 mm and intermediate length of 150 mm. The load was applied by a universal testing machine (UTM), which has the load capacity up to 500 kN, with the loading rate of 0.001mm/minute. The UHPFRC specimens avoided any brutal fracturing and showed a tension-stiffening behavior. The tensile strengths of the mixtures are shown in Table 2. The steel fibers prevented little cracks from growing. After the first crack, the UHPFRC will be able to take more tensile stress. The tensile strength of the UHPFRC groups increased by 51.2% to 224.2% over plain concrete groups. The tensile-compressive strength ratio ranged from 1:41.8 to 1:17.8. The tensile strength improved significantly as the volume of steel fibers increased from 0.5% to 2%.

The UHPFRC beams with dimensions of 100 ×100 × 400 mm were fabricated for the four-point flexural tests which were performed to obtain the flexural curves. The space between load points is 1/3 of the clear span length where a region of no shear generates. The loading mode is displacement control, with the loading rate of 0.1 mm/minute. The deflection is measured by linear variable differential transformer (LVDT) located at the mid-span of the specimen. The UHPFRC beams exhibited post-crack stiffening behavior and ductility in flexural tests. The specimen of group UHPFRC4 can be used as an example to demonstrate the damage process. Before the cracking load, the curve of the specimen was practically linear. The loading stiffness decreased after many flexural cracks appeared in the middle of the UHPFRC beam, and the width of flexural cracks did not continue to increase uncontrollably due to the steel fibers. At the maximum load, the major flexural crack formed, the steel fibers were pulled out, and squeaking was heard. The flexural strengths of the test beams are presented in Table 2. The flexural strengths of UHPFRC beams improved as the volume of steel fibers increased. Compared to UHPFRC0, the flexural strengths of UHPFRC2, UHPFRC4, and UHPFRC6 increased by 108.3%, 206.2%, and 286.9%, respectively. The load-deflection curves of different groups are shown in Fig. 2. The toughness is the most desired property of the concrete, which characterizes the capacity of material to energy absorption. The toughness is evaluated by determining the area under load-deflection curve up to a deflection of 1/150 of the clear span length (ASTM C1609-12, 2012). Compared to UHPFRC2, the toughness of UHPFRC4 and UHPFRC6 increased by 60.9.%, and 112.3%, respectively. The toughness is presented in Table 2.

3. Experimental Program

3.1 Detail of the specimens

The experimental study had seven specimens: one HSC column and six UHPFRC columns. The height of specimens were 1000 mm, and the square cross-section was 150 × 200 mm. The test variables were the load eccentricity,

Table 2 Material test results

Groups	Slump Flow/mm	Compressive Strength/MPa	Tensile Strength/MPa	Flexural Strength/MPa	Toughness/J
UHPFRC0	290	105.3	2.52	4.95	-
UHPFRC1	281	112.4	3.81	8.57	48.70
UHPFRC2	269	118.6	4.63	10.31	57.48
UHPFRC3	251	127.5	5.21	12.99	67.60
UHPFRC4	236	134.0	6.35	15.16	78.34
UHPFRC5	210	140.8	7.23	17.08	88.96
UHPFRC6	192	145.2	8.17	19.15	100.38

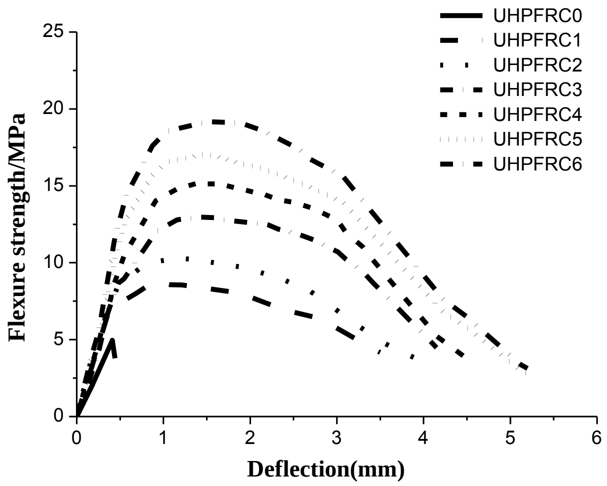

Fig. 2 Load-deflection curves of flexural tests

volume of steel fibers, and stirrup ratio. To prevent a local compression failure, the specimens were strengthened at the ends with four rows of reinforcement mesh (40 mm apart). The longitudinal reinforcement ratio of all specimens was 1.03%. The design parameters of columns are shown in Table 3, Specimens were symmetrically reinforced and designed with identical shapes and sizes, as shown in Fig. 3.

Each cube meter of the high-strength concrete was mixed with 210 kg of water, 490 kg of cement, 797 kg of natural coarse aggregate, 742 kg of natural fine aggregate, 70 kg of fly ash, 66 kg of silica fume, and 25 kg of super-plasticizer. Table 4 shows the mechanical properties results of concrete. The prism compressive strength (f_c) and elastic modulus (E_c) of concrete were defined as the prism specimens with dimensions of 100 ×100 ×300 mm. Reinforcements conforming to D16 (16 mm diameter) were used for the longitudinal reinforcements, while those conforming to D8 (8 mm diameter) were used for the stirrups. For each type of reinforcements, three standard test samples were prepared for the tensile tests. The means of yield strength and ultimate strength for reinforcement of D16 were 472 MPa and 617 MPa, and the corresponding figures for reinforcement of D8 were 568 MPa and 723 MPa, respectively.

3.2 Test setup and measurement arrangement

All specimens were tested under uniaxial compression using a 5000-kN electro-hydraulic servo testing machine, as shown in Fig. 4(a). The knife edge hinge support was set

Table 3 Design parameters of specimens

Specimens	H×h×b/mm	V_f/%	e_0/mm	ρ_v %
HSCZ-1	1000×200×150	0%	100	2.01%
UHPFRCZ-1	1000×200×150	1%	100	2.01%
UHPFRCZ-2	1000×200×150	2%	100	2.01%
UHPFRCZ-3	1000×200×150	2%	100	1.34%
UHPFRCZ-4	1000×200×150	1%	40	2.01%
UHPFRCZ-5	1000×200×150	2%	40	2.01%
UHPFRCZ-6	1000×200×150	2%	40	1.34%

* H is the height of the specimen, h is the height of the specimen cross-section, b is the width of the specimen cross-section, V_f is the volume of steel fibers, e_0 is the load eccentricity, and ρ_v is the stirrup ratio.

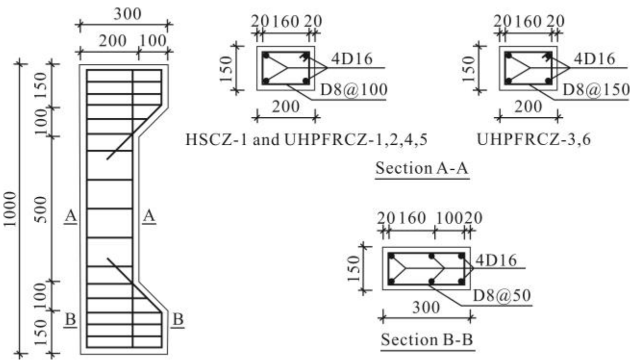

Fig. 3 Reinforcement configuration of specimens

Table 4 Mechanical properties of concrete

Groups	V_f/%	f_c/MPa	f_t /MPa	E_c/10^4MPa
HSC	0	81.3	2.9	3.7
UHPFRC	1%	103.8	5.2	4.2
	2%	117.8	7.1	4.3

*f_c and f_t are the load values when that decreases to 85% load at peak point.

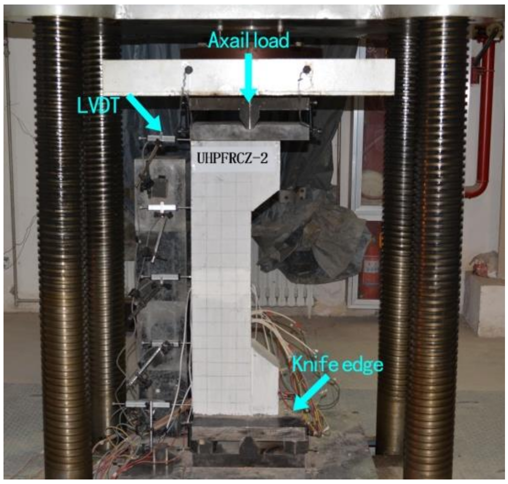

(a) Test setup

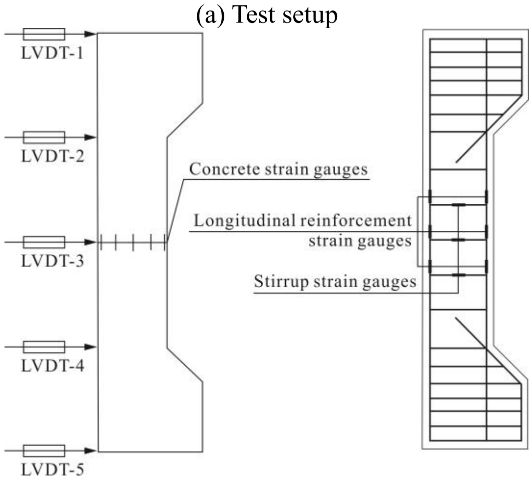

(b) Measurement arrangement

Fig.4 Test Setup and measurement arrangement

between the ends of the specimens and the press plate of the testing machine to simulate the hinge connection. In the test, a predetermined axial compressive load was applied to examine the working performance. A displacement control approach with a rate of 0.2 mm/min was used for the test specimens. It was considered the displacement control can continue the post-peak load stage.

The load values, midspan deflections, reinforcement strains, concrete strains, and width of cracks were measured. The load values were measured by the electro-hydraulic servo testing machine. Five horizontal linear variable different transformers (LVDTs), 250 mm apart from each other, were arranged to measure the midspan deflection of the columns. The LVDTs had the operating range of ±20 mm. The vertical deformation is measured by the displacement sensor in the electro-hydraulic servo testing machine. Three strain gauges were arranged on longitudinal reinforcement, and one of those was placed in the midpoint and the other two were placed 100mm apart from the midpoint one. Six strain gauges were arranged on the three stirrups. The concrete strain gauges were arranged in the middle of the columns. The arrangement of the strain gauges and LVDTs is shown in Fig. 4(b). A crack-observation instrument was used to measure the width of cracks. All test data were collected using a DH3816N data-acquisition system.

4. Experimental results

4.1 Crack patterns and failure modes

Base on the observed crack pattern of tested columns, the failure modes were found to depend on the load eccentricity, which is presented in Fig. 5.

HSCZ-1 was the high-strength concrete large eccentric compression column. When the load was approximately 0.25 N_c (the calculated peak load), horizontal visible cracks appeared in the tension zone. With the increased load, the horizontal cracks quickly widened. When the load reached approximately 0.75 N_c, the tensile longitudinal reinforcement yielded and vertical cracks appeared in the compression zone. After peak load, a large area of the HSC was spalling and crushing in the middle of the column. Fig. 5(a) shows the specimen failure mode.

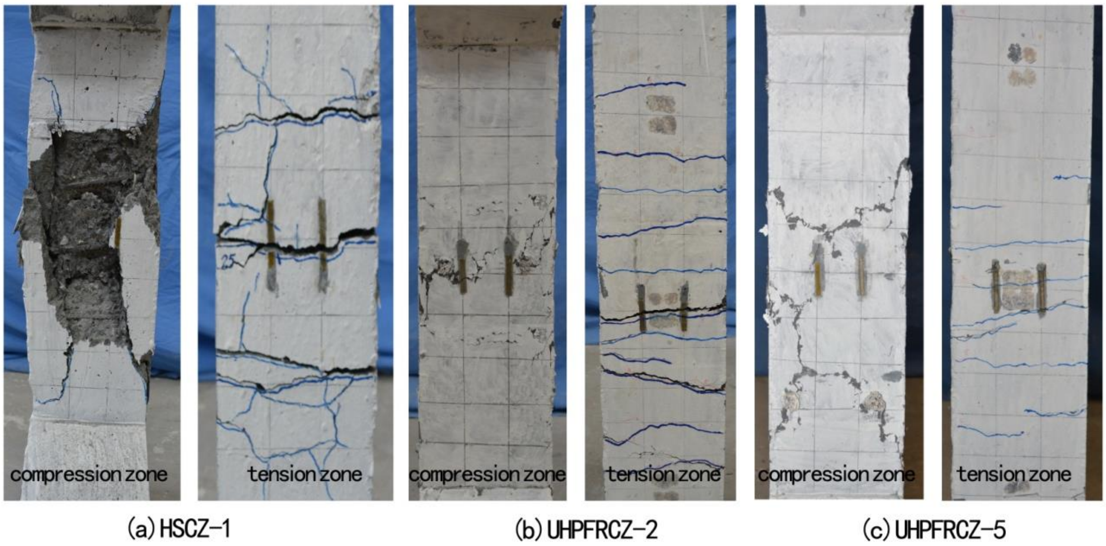

Fig. 5 Failure modes of (a) HSCZ-1 (b) UHPFRCZ-2 (c) UHPFRCZ-5

UHPFRCZ-1, UHPFRCZ-2, and UHPFRCZ-3 were large eccentric compression columns. When the load was approximately 0.3 N_c, horizontal micro-cracks appeared in the tension zone of the columns. The number of cracks gradually increased and new cracks developed between the existing ones, but the width of cracks slowly developed due to the fiber bridge effect. As the load was approximately 0.78 N_c, the tensile reinforcement yielded and the number of cracks in the tension zone continued to increase. Then, the vertical cracks appeared in the compression zone of the columns and the width of horizontal cracks gradually increased. The steel fibers started to be pulled out from the concrete. After the peak load, diagonal cracks could be seen in the compression zone, and the UHPFRC cover peeled off. The failure mode is shown in Fig. 5(b). The cracks of the UHPFRCZ columns were denser and narrower in the tension zone. The spalled area was found to be significantly smaller compared to HSCZ column because of the bridging effect of steel fibers. Moreover, the cracks of UHPFRCZ-3 were more concentrated and rapidly widening than those of UHPFRCZ-1 and UHPFRCZ-2 in the tension zone.

UHPFRCZ-4, UHPFRCZ-5, and UHPFRCZ-6 were small eccentric compression columns. In the initial stage, cracks did not appear on the surface of specimens. When the load was approximately 0.8 N_c, slight vertical tensile cracks and horizontal compressive cracks appeared. Then the compressive strains of UHPFRC rapidly increased, and the vertical cracks of the columns rapidly widened in the compression zone. Up to approximately 0.95 N_c, significant vertical cracks were formed in the middle of the columns, and horizontal cracks did not develop in the tension zone. As the peak load was reached, the UHPFRC cover was crushing, and several obvious vertical cracks formed. The failure mode is shown in Fig.5(c). Compared with UHPFRCZ-4, UHPFRCZ-5 showed a greater range of damage and better ductility, and UHPFRCZ-6 presented a more rapid development of vertical cracks.

The observations justified that the failure mode of eccentric compression UHPFRC columns can be defined as tension failure and compression failure. The use of UHPFRC changes the typical failure mode observed in HSC columns. Because of the steel fibers, the HSC column brittle failure mode was changed to UHPFRC columns ductility failure mode. The UHPFRC columns showed damage-control properties, and no significant large concrete fragmentations are observed.

4.2 Load-deflection response

The axial load-midspan deflection curves are shown in Fig. 6, which of deflection is obtained by the middle LVDT. The curves of the large eccentric compression columns are shown in Fig. 6(a). The slopes of curves were linearly developed in the elastic stage. With the tensile longitudinal reinforcements yielded, the specimens were transformed to the yielding stage, with turning points as shown on the curves. The specimens continued to gain load, but the behavior was characterized by a reduced stiffness as the horizontal crack widths gradual grew. The curve of HSCZ-1 showed an inflection point and load-carrying capacity subsequently decreased sharply after the peak load, indicating that the deformation of the specimen was poor. However, the stiffness of UHPFRC, slowly decreased as the steel fibers significantly affected the deflection development of columns. The deflection improved with the increase in the volume of steel fibers and stirrup ratio. The load-midspan deflection curves of the small eccentric compression columns are shown in Fig. 6(b). Before the peak load, the curves were approximately straight. The curves then showed a turning point at peak load. The vertical crack widths and mid-span deflection grew larger. The curves for the small eccentric compression columns had a steeper descending, indicating that the deformation of UHPFRC small eccentric compression columns was less than that of large eccentric compression columns.

4.3 Bearing capacity and deformation

The test loads of the specimens are shown in Table 5. The peak load was used to reflect the bearing capacity of

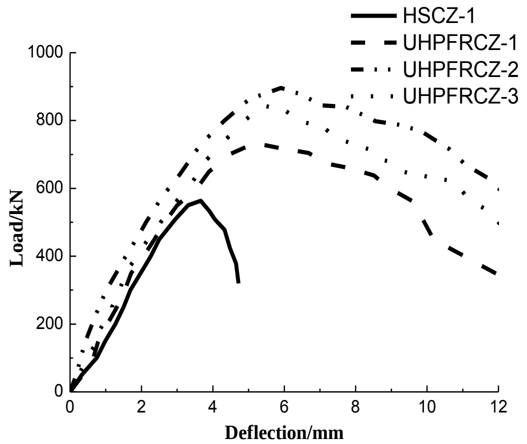

(a) Large eccentric compression

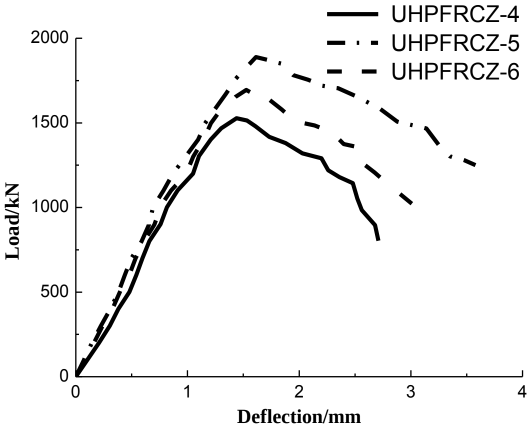

(b) Small eccentric compression

Fig. 6 Load-deflection curves

Table 5 Test results of bearing capacity and deflections

Specimens	N_{ck} /kN	N_t /kN	Δ_p /mm	Δ_u /mm	θ
HSCZ-1	141.1	563.2	3.7	4.3	0.0076
UHPFRCZ-1	203.9	733.3	5.2	8.2	0.0164
UHPFRCZ-2	265.4	895.5	5.9	10.6	0.0212
UHPFRCZ-3	251.7	843.2	5.4	9.3	0.0186
UHPFRCZ-4	839.0	1527.7	1.4	2.2	0.0044
UHPFRCZ-5	950.5	1889.1	1.6	2.7	0.0054
UHPFRCZ-6	944.6	1696.6	1.5	2.3	0.0046

*N_{ck} is cracking load, N_t is peak load, Δ_p is the deflection corresponds to peak load, Δ_u is the ultimate deflection corresponds to the load decreased to 85% of the peak load. θ is the ultimate deflection ratio defined as $2\Delta_u /H$.

the columns. The cracking load and peak load were improved with increasing in the volume of steel fibers. The highest improvement in the cracking load and peak load was observed for UHPFRCZ-2, Compared with HSCZ-1, the cracking load and peak load of UHPFRCZ-2 increased 88.1% and 58%. Also, the cracking load and peak load of UHPFRCZ-5 increased by 13.3% and 23.7%, respectively, compared to UHPFRCZ-4. The stirrup ratio affected the peak load but hardly affected the cracking load with the same volume of steel fibers. The peak load of UHPFRCZ-2 was 6.2% higher than that of UHPFRCZ-3, and the peak load of UHPFRCZ-5 increased by 11.4% compared to UHPFRC-6. The midspan deflection of the columns is used to reflect their deformation. The test results are shown in Table 5. It was observed that the load eccentricity and volume of steel fibers obviously affected the deflection of the columns. For the deflections of large eccentric compression columns, the ultimate deflections increased by 90.7%, 146.5% and 116.3%, respectively, compared with HSCZ-1. The peak deflection and ultimate deflection of UHPFRC-5 increased by 14.3% and 29.4%, respectively, compared with UHPFRCZ-4. If the volume of steel fibers was identical, the ultimate deflections were improved with the increase in the stirrup ratio. The ultimate deflection of UHPFRCZ-2 was 14% higher than that of UHPFRCZ-3, and the ultimate deflection of UHPFRC-5 was 17.4% higher than that of UHPFRCZ-6. The UHPFRC columns showed higher enhancement in the bearing capacity and deformation due to the micro steel fibers produced more effective reinforcing mechanisms.

4.4 Reinforcement strain analysis

The relationship between axial load and longitudinal reinforcement strains is illustrated in Fig. 7. For the large eccentric compression columns, the load-strain curves were in a linear relationship before the tensile longitudinal reinforcements yielded. As the load increased continuously, the strains increased quickly. The slope of the load-strain curves for UHPFRC columns decreased more slowly. The largest strains were observed in the middle of columns across the main horizontal cracks. The longitudinal reinforcements of the UHPFRC columns had higher strain values than HSC column. The compressive longitudinal reinforcements of the small eccentric compression columns also displayed a linear relationship between the load and strains before compressive longitudinal reinforcements yielded. The strains then developed quickly compared to that of the tensile longitudinal reinforcements. The specimens can reach the higher strain values with the increase of stirrup ratio. No yield in the longitudinal reinforcements were measured in tension zone of small eccentric compression columns.

5. Numerical simulation

The nonlinear finite element (FE) analysis was used to simulate the damage process and better understand the eccentric compression behavior of the UHPFRC column. FE analyses results were conducted to compare with the experimental results. The FE analysis software used for the analytical studies was ABAQUS (2011). The structural geometry, boundary conditions and relevant material modes were described.

5.1 Material modeling

The stress-strain relationship of longitudinal reinforcement and stirrup was the idealized elastic-plastic model, and more detail of this stress-strain relation can be

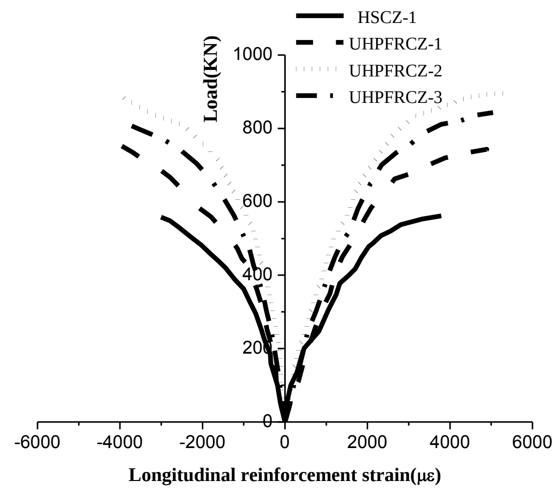

(a) Large eccentric compression

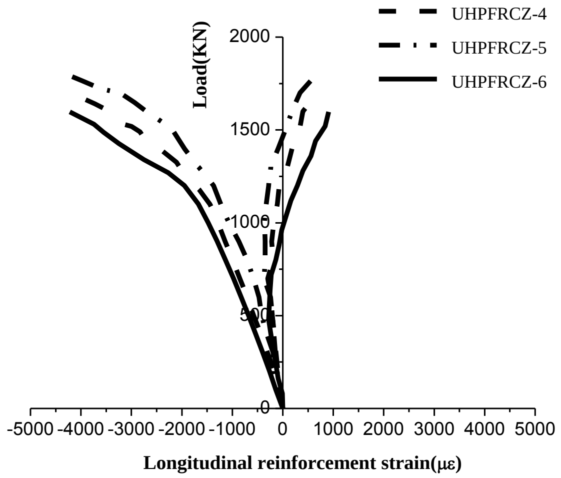

(b) Small eccentric compression

Fig. 7 Load-strain curves

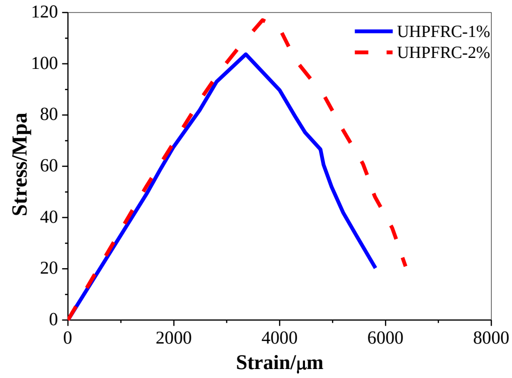

(a) Compression

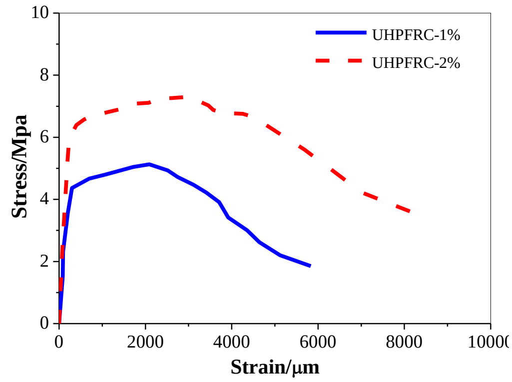

(b) Tension

Fig. 8 Stress-strain relation of concrete

found (Belarbi, *et al.* 1994). The Poisson ratio was taken as 0.3. The UHPFRC is modeled as a homogeneous material and the fibers are uniformly distributed in the mixture. The concrete damage plastic model (CDPM) was selected to simulate the damage progress of concrete. Compression crushing and tensile cracking of concrete were considered in CDPM. The inelastic and fracture behaviour of concrete were presented by the concept of isotropic damage evolution, which take isotropic tensile and compressive plasticity into account. Because CDPM introduced the damage index into the concrete model, the elastic stiffness matrix of the concrete is reduced. The damage index or the material stiffness degradation index varies from 0 representing no damage to 1 representing complete failure. The CDPM is defined by five other parameters: the ratio of initial equibiaxial compressive yield stress to initial uniaxial compressive yield stress, the ratio of the second stress invariant on the tensile meridian to that on the compressive meridian, the flow potential eccentricity, the viscosity parameter and the dilation angle in degrees. The default values were used herein, which were 1.16, 0.0, 0.1, 0.66 and 35^{o} respectively. The compression and tension stress-strain relationships of UHPFRC with different volume of steel fibers are defined in Fig. 8.

5.2 Element contact properties and boundary conditions

The UHPFRC was modeled with three-dimensional 8-node solid elements (C3D8R). The three-dimensional 2-node truss element (T3D2) was modeled for longitudinal reinforcement and stirrups. This element is a long, slender structural member that transmits only axial load. The accuracy of the FEM analysis and the computational time and stability are highly depending on the model configuration and FEM mesh. Assuming perfect bond, embed constraint was used to stimulate the reinforcements and UHPFRC columns to reduce the computation time. The mesh size of solid element was 25mm to guarantee calculation accuracy. The further decrease in mesh size had insignificant affection on the accuracy of results. The vertical load was applied to the top of the columns. The boundary conditions for all the columns were identical and consisted of pin support at the top and bottom of the specimens, The columns were analyzed in displacement control to simulate the eccentric compression behavior.

5.3 Comparison of experimental and analytical results

The numerical results for UHPFRC columns in terms of load-deflection response are shown in Fig. 9. The FE analysis models were able to simulate the experimental loading process closely. The initial stiffness of the FE models was slightly higher than the actual test specimens.

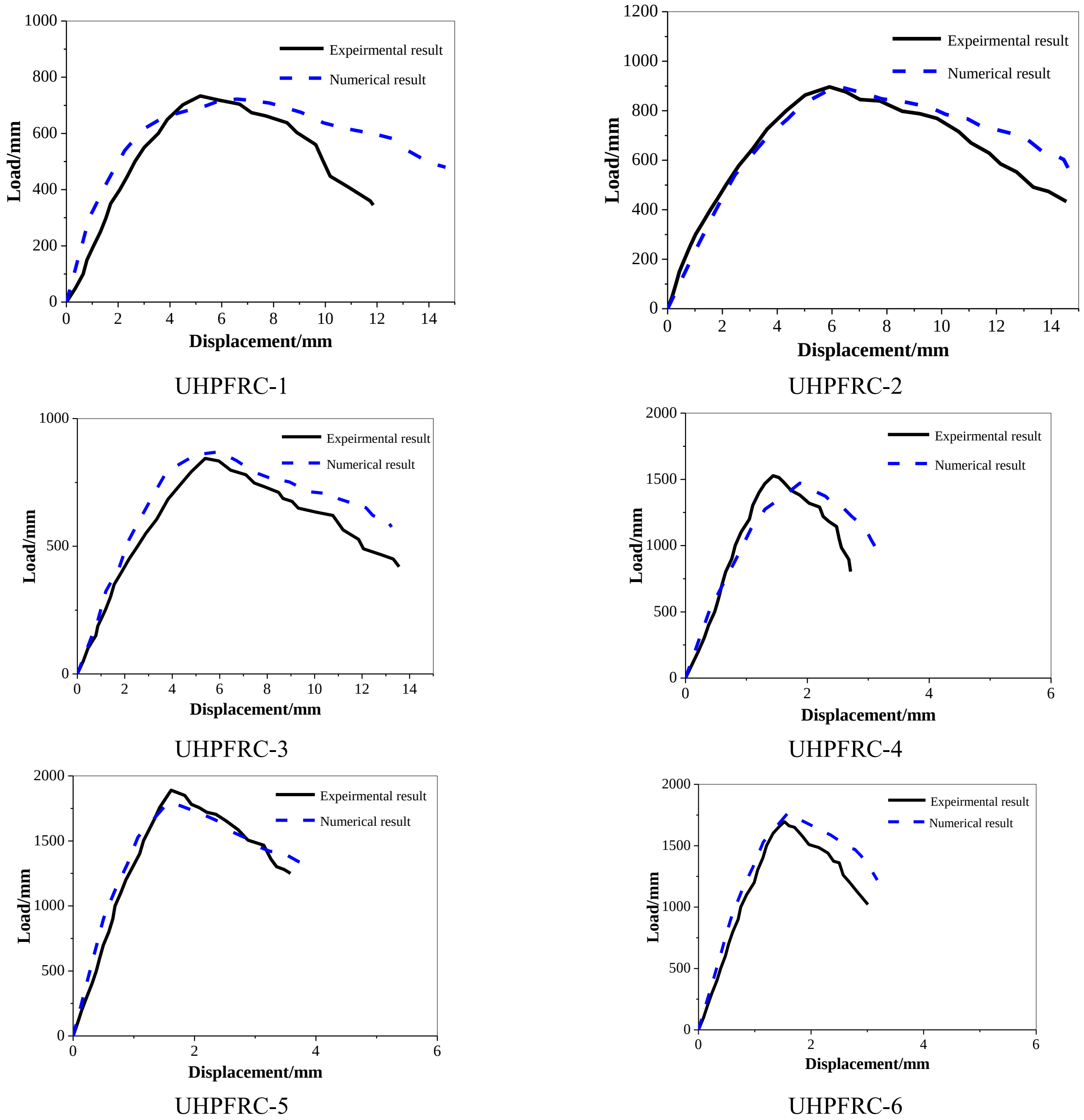

Fig. 9 Load-deflection behaviors of experiment results and FE analysis

The reason might be mainly attributed to assume material properties from the actual properties, and perfect bonding between the reinforcement and concrete. Fig.10 shows the damage pattern and compares the FE analysis and experimental results at the maximum load. The FE model of large eccentric compression UHPFRC column presented multiple crack patterns. The failure modes from the FE analysis agree well with the experimental results.

6. Predicted of bearing capacity

6.1 Large eccentric compression UHPFRC columns

Because of the high tensile strength of UHPFRC, the contribution of the UHPFRC tensile strength is considered in the bearing capacity formulas. The equivalent stress distributions of the specimens are shown in Fig. 11. The large eccentric compression UHPFRC columns had symmetric reinforcement, so $A_S = A_S'$ and $f_S = f_S'$. According to the test results, all longitudinal reinforcements yielded. The following equations are established:

$$C = \alpha f_c b \beta x \tag{1}$$

$$T_s = T_s' = f_s A_s \tag{2}$$

$$T_c = k f_t b (h - x) \tag{3}$$

$$N_c = C - T_c \tag{4}$$

$$N_c (e_0 + 0.5h) = C(h - 0.5\beta x) + T_s'(h - a_s') - 0.5T_c(h - x) - T_s a_s' \tag{5}$$

(a) UHPFRCZ-3 (b) UHPFRCZ-6

Fig. 10 Cracking pattern of experiment results and FE analysis

where x is the length of the UHPFRC compression zone; f_y and A_s are the yield strength and cross-section area of longitudinal reinforcements in the compression zone, respectively; a_s and a_s' is the distance between the edge of the column and the longitudinal reinforcements of the compression and tension; α and β is the equivalent stress distribution magnitude and length and index of the compression zone; which are defined as α = 0.90 and β = 0.71 (MHSURDC 2010). k is the equivalent stress distribution index of the tension zone. Based on equations (1) and (2), k can obtain

$$k = \frac{C(h-0.5\beta x) - N_c(e_0+0.5h) + T_s'(h_0 - 2a_s')}{0.5 f_t b\left(h-x\right)^2} \tag{6}$$

The test data of UHPFRC large eccentric compression columns and flexure beams were collected and calculated (Yang *et al.* 2010, Yoo and Yoon 2015, Qi *et al.* 2017, Singh *et al.* 2017). The calculated results are shown in Fig. 12. The mean value is k = 0.45, and the standard deviation is 0.094. For safety considerations, the value k = 0.40 is used.

6.2 Small eccentric compression UHPFRC columns

Since the length of the tension zone is small, the contribution of the UHPFRC tensile strength was ignored in the bearing capacity calculation formulas of small eccentric compression columns. The equivalent stress distributions of the specimens are shown in Fig. 11. The following equations are established:

$$C = \alpha f_c b \beta x \tag{7}$$

$$T_s = E_s \varepsilon_{cu}\left(\frac{h-a_s}{x} - 1\right) A_s \tag{8}$$

$$T_s' = f_s' A_s' \tag{9}$$

$$N_c = C + T_s' - T_s \tag{10}$$

$$N_c(e_0+0.5h) = C\left(h-0.5\beta x\right) + T_s'\left(h-a_s'\right) - T_s a_s' \tag{11}$$

Where, ε_{cu} is the ultimate compressive strain of UHPFRC, as the compressive stress can be taken as a constant value of $0.85 f_{cu}$.

Table 6 Comparison of calculated and experimental results

Specimens	N_c /kN	N_{FE}	N_t /kN	N_c / N_t	N_{FE} / N_t
UHPFRCZ-1	718.6	727.4	733.3	0.98	0.99
UHPFRCZ-2	841.2	894.3	895.5	0.94	1.00
UHPFRCZ-3	841.2	870.2	843.2	0.99	1.03
UHPFRCZ-4	1465.3	1472.5	1527.7	0.96	0.96
UHPFRCZ-5	1668.4	1804.8	1889.1	0.88	0.96
UHPFRCZ-6	1668.4	1760.2	1696.6	0.98	1.04

6.3 Comparison of test values with calculated values

The results are shown in Table 6. The mean value of N_c/ N_t is 0.955. The calculated values are good agreement with the experimental values. The calculation method provides a theoretical basis for engineering applications.

7. Conclusions

This paper presents research on the mechanical properties of UHPFRC and eccentric compression behavior of UHPFRC columns. The test variables included load eccentricity, volume of steel fibers and stirrup ratio. The following conclusions can be drawn:

(1) The flowability values decreased obviously as the volume of steel fibers increased. The UHPFRC had high compressive, tensile, and flexural strength. The volume of steel fibers of 2% is advised for the column test.

(2) Eccentric compression UHPFRC columns can be defined as different failure modes. The large eccentric

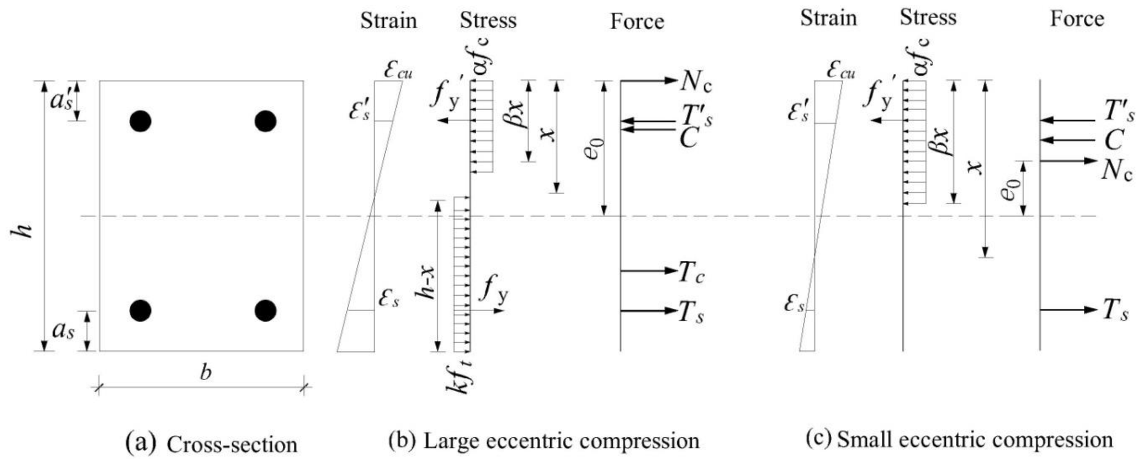

Fig. 11 Stress and strain distribution of specimens

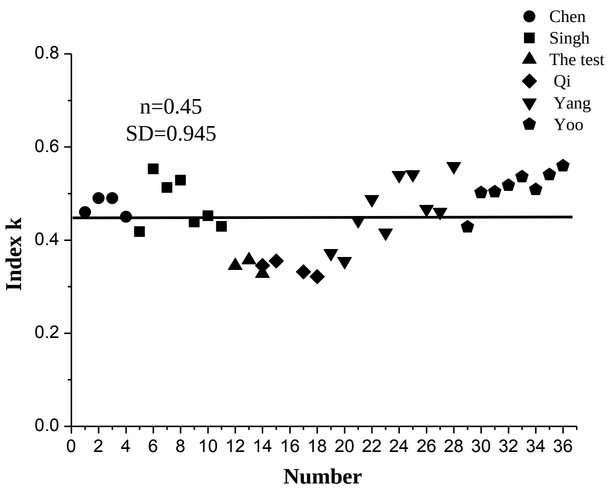

Fig. 12 Scatter plot of equivalent coefficient

compression failure mode was the yielding of the longitudinal tensile reinforcement, and multiple horizontal cracks appeared in the tension zone. The small eccentric compression failure mode was that the yielding of the longitudinal compressive reinforcement and the vertical cracks appeared in the compressive zone.

(3) The cracking load, peak load, and ultimate deflection of UHPFRC columns increased significantly as the volume of steel fibers increased. The stirrup ratio improved the bearing capacity and deformation of small eccentric compression UHPFRC columns. The large eccentric compression columns showed better deformation.

(4) The FE models were able to simulate the damage process of the UHPFRC columns. The results of finite element modelling (FEM) showed good agreement with the experimental test results. The numerical tool is used to simulate eccentric compression UHPFRC columns efficiently.

(5) The calculation formulas of bearing capacity considered the contribution of the UHPFRC tensile strength have been obtained. The calculation results were consistent with the test results.

Acknowledgements

This research was financially supported by the National Natural Science Foundation of China (Grant No.51308052), Natural Science Foundation of Shanxi Province (Grant No.2017JM037) and Supported by the Fundamental Research Funds for the Central Universities, CHD. The financial support is gratefully acknowledged.

References

Abaqus 6.11 (2011), *Abaqus Analysis User's Manual Dassault Systemes*, Hibbit, Karlsson and Sorensen. Inc., RI, USA.

AFGC (Association Française du Génie Civil) (2013), *Ultra High Performance Fibre-Reinforced Concretes*, AFGC, Bagneux, France.

Al-Osta M.A., Isa, M.N. and Baluch, M.H. (2017), "Flexural behavior of reinforced concrete beams strengthened with ultra-high performance fiber reinforced concrete", *Construct. Build. Mater.*, **134**(3), 279-296. https://doi.org/10.1016/j.conbuildmat.2016.12.094.

ASTM C1609-12. (2012), *Standard Test Method for Flexural Performance of Fiber-Reinforced Concrete (Using Beam with Third-Point Loading)*, ASTM International, West Conshohocken, USA.

Belarbi, A. and Hsu, T.T.C. (1994), "Constitutive laws of concrete in tension and reinforcing bars stiffened by concrete", *ACI Struct. J.*, **91**(4), 465-474.

Alsalman, A., Dang, C.N. and Hale, W.H. (2017), "Development of ultra-high performance concrete with locally available materials", *Construct. Build. Mater.*, **133**(2), 135-145. https://doi.org/10.1016/j.conbuildmat.2016.12.040.

Chen, S.M., Zhang, R., Jia, L.J. and Wang, J.Y. (2018), "Flexural behaviour of rebar-reinforced ultra-high performance concrete beams", *Mag. Concrete Res.,* https://doi.org/10.1680/jmacr.17.00283.

CSTCC (Chinese Standardization Technical Committee of Concrete) (2015), "Reactive powder concrete", GB/T 31387-2015; China Stand Press, Beijing, China.

Fehling, E., Schmidt, M., Walraven, J., Leutbecher, T. and Fröhlich, S. (2014), *Ultra-High Performance Concrete UHPC: Fundamentals, Design, Examples*, Ernst and Sohn, Berlin, Germany.

FHWA (2013), "Ultra-high performance concrete: A state-of-the-art report for the bridge community", FHWA-HRT-13-060; FHWA, Washington, DC, USA.

Graybeal, B.A. (2007), "Compressive behavior of ultra-high performance fiber reinforced concrete", *ACI Mater. J.*, **104**(2), 146-152.

Habel, K., Viviani, M., Denarié, E. and Brühwiler, E. (2006), "Development of the mechanical properties of an ultra-high performance fiber reinforced concrete", *Cement Concrete Res.*, **36**(7), 1362-1370. https://doi.org/10.1016/j.cemconres.2006.03.009.

Heinz, D., Urbonas, L. and Gerlicher, T. (2012), "Effect of heat treatment method on the properties of UHPC", *Proceedings of Hipermat 3rd International Symposium on UHPC and Nanotechnology for High Performance Construction Materials*, Kassel, Germany, March.

Hoang, A.L. and Fehling, E. (2017), "Influence of steel fiber content and aspect ratio on the uniaxial tensile and compressive behavior of ultra-high performance concrete", *Construct. Build. Mater.*, **153**(10), 790-806. https://doi.org/10.1016/j.conbuildmat.2017.07.130.

Hosinieh, M.M. and Aoude, H. (2015), "Behavior of ultra-high performance fiber reinforced concrete columns under pure axial loading", *Eng. Struct.*, **99**(9), 388-401. https://doi.org/10.1016/j.engstruct.2015.05.009.

Hu, A.X., Yu, J., Liang, X.W. and Shi, Q.X. (2018), "Tensile characteristics of ultra-high-performance concrete", *Mag. Concrete Res.*, **70**(6), 314-324. https://doi.org/10.1680/jmacr.17.00126.

JSCE (Japan Society of Civil Engineers) (2006), "Recommendations for design and construction of ultra-high strength fiber reinforced concrete structures (Draft)", JSCE, Tokyo, Japan.

KCI (Korea Concrete Institute) (2012), *KCI-M-12-003: Design Recommendations for Ultra-high Performance Concrete*, Korea Concrete Institute, Seoul, Korea.

Kazemi, S., and Lubell, A.S. (2012), "Influence of specimen size and fiber content on mechanical properties of ultra-high-performance fiber-reinforced concrete", *ACI Mater. J.*, **109**(6), 75-684.

Larrard, F., and Sedran, T. (1994), "Optimization of ultra-high performance concrete by the use of a packing model", *Cement Concrete Res.*, **24**(6), 997-1009. https://doi.org/10.1016/0008-8846(94)90022-1.

Lubliner, J., Oliver, J., Oller, S., and Oñate, E. (1989), "A plastic-damage model for concrete", *J. Solids Struct.*, **25**(3), 299-326. https://doi.org/10.1016/0020-7683(89)90050-4.

Magureanu, C., Sosa, I., Negrutiu, C. and Heghes, B. (2012), "Mechanical properties and durability of ultra-high-performance concrete", *ACI Mater. J.*, **109**(2), 177-184.

MHURDC (Ministry of Housing and Urban-Rural Development of China) (2010), "Code for design of concrete structures", GB50010-2010; Chinese Architecture and Building Press, Beijing, China.

Qi, J.N., Ma, Z.J. and Wang, J.Q. (2017), "Flexural response of high-strength steel-ultra-high-performance fiber reinforced concrete beams based on a mesoscale constitutive model: Experiment and theory", *Struct. Concrete*, **19**(3), 1-16. http://doi.org/10.1002/suco.201700043.

Murthy, A.R., Aravindan, M. and Prakasam, G. (2018), "Prediction of flexural behaviour of RC beams strengthened with ultra-high performance fiber reinforced concrete", *Struct. Eng. Mech.,* **65** (3), 315-325. https://doi.org/10.12989/sem.2018.65.3.315.

Richard, P. and Cheyrezy, M. (1995), "Composition of reactive powder concretes", *Cement Concrete Res.*, **25**(7), 1501-1511. https://doi.org/10.1016/0008-8846(95)00144-2.

Rossi, P. (2001) "Ultra high-performance concrete", *Concrete*, **23**(12), 46-52.

Safdar, M., Matsumoto, T. and Kakuma, K. (2016), "Flexural behavior of reinforced concrete beams repaired with ultra-high performance fiber reinforced concrete (UHPFRC)", *Compos. Struct.*, **157**(11), 448-460. https://doi.org/10.1016/j.compstruct.2016.09.010.

Schachinger, I., Hilbig, H. and Stengal, T. (2008), "Effect of curing temperatures at an early age on the long-term strength development of UHPC", *Proceedings of the Second International Symposium on Ultra High Performance Concrete*, Kassel, Germany, March. 205-212.

Shin H.O., Min, K.H. and Mitchell, D. (2017), "Confinement of ultra-high performance fiber reinforced concrete columns", *Compos. Struct.*, **176**(9), 124-142. https://doi.org/10.1016/j.compstruct.2017.05.022.

Singh, M., Sheikh, A.H. and Ali, M.S.M. (2017), "Experimental and numerical study of the flexural behavior of ultra-high performance fibre reinforced concrete beams", *Construct. Build. Mater.*, **8**(5), 12-25. https://doi.org/10.1016/j.conbuildmat.2017.02.002.

Su, Y., Wu, C.Q. and Li, J. et al (2017), "Development of novel ultra-high performance concrete: from material to structure", *Construct. Build. Mater.*, **135**(3), 517-528. https://doi.org/10.1016/j.conbuildmat.2016.12.175.

Prem, P.R., Murthy, A.R. and Bharatkumar, B.H. (2015), "Influence of curing regime and steel fibres on the mechanical properties of UHPC", *Mag. Concrete Res.*, **67**(18), 988-1002. http://dx.doi.org/10.1680/macr.14.00333.

Wang, C., Yang, C. and Liu, F. (2012), "Preparation of ultra-high performance concrete with common technology and materials", *Cement Concrete Compos.*, **34**(2), 538-544. https://doi.org/10.1016/j.cemconcomp.2011.11.005.

Wu, Z., Shi, C., He, W. and Wu, L. (2016), "Effects of steel fiber content and shape on mechanical properties of ultra-high performance concrete", *Construct. Build. Mater.*, **103**(1), 8-14. https://doi.org/10.1016/j.conbuildmat.2015.11.028.

Xu, S.C., Wu, C.Q. and Liu, Z.X. (2017), "Experimental investigation of seismic behavior of ultra-high performance steel fiber reinforced concrete columns", *Eng. Struct.*, **152**(12), 129-148. https://doi.org/10.1016/j.engstruct.2017.09.007.

Yang I.H., Joh C.B. and Kim, B.S. (2012), "Flexural response predictions for ultra-high performance fibre reinforced concrete beams", *Mag. Concrete Res.*, **64**(2), 113-127. https://doi.org/10.1680/macr.10.00115.

Yoo, D.Y. and Yoon, Y.S. (2015), "Structural performance of ultra-high performance concrete beams with different steel fibers", *Eng. Struct.*, **102**(11), 409-423. https://doi.org/10.1016/j.engstruct.2015.08.029.

Yoo, D.Y. and Yoon, Y.S. (2016), "A review on structural behavior, design, and application of ultra-high-performance fiber-reinforced concrete", *J. Concrete Struct. Mater.*, **10**(2), 125-142. https://doi.org/10.1007/s40069-016-0143-x.

Yu, R., Spiesz, P. and Brouwers, H.J.H. (2015), "Development of an eco-friendly Ultra-high performance concrete with efficient cement and mineral admixtures uses", *Cement Concrete Compos.,* **55**(1), 383-394. https://doi.org/10.1016/j.cemconcomp.2014.09.024.

CC